Electronic Supporting Information

for

Reversible dioxygen binding on asymmetric dinuclear rhodium centres

Takayuki Nakajima,* Miyuki Sakamoto, Sachi Kurai, Bunsho Kure, Tomoaki Tanase*

Department of Chemistry, Faculty of Science, Nara Women's University, Kitauoya-higashi-machi, Nara 630-8506, Japan.
Fax: +81 742 203847; Tel: +81 742 203399; E-mail: tanase@cc.nara-wu.ac.jp

Experimental and spectral data for complexes 1a–c and **2a–d**

Table S1. Crystallographic Data of Complexes **1a**·3CH_2Cl_2, **1b**·2Me_2CO, **2c**·4MeCN and **2d**·CH_2Cl_2
Table S2. Structural Parameters of **1a**, **1b**, **2c** and **2d**.
Figure S1. ORTEP diagram for **1b** with the atomic numbering scheme.
Figure S2. ORTEP diagram for **2c** with the atomic numbering scheme.
Figure S3. ESI-TOF-MS spectra of **1a** in CH_2Cl_2.
Figure S4. ESI-TOF-MS spectra of **1b** in CH_2Cl_2.
Figure S5. ESI-TOF-MS spectra of **1c** in CH_2Cl_2.
Figure S6. ESI-TOF-MS spectra of **2a** in CH_2Cl_2.
Figure S7. ESI-TOF-MS spectra of **2b** in CH_2Cl_2.
Figure S8. ESI-TOF-MS spectra of **2c** in CH_2Cl_2.
Figure S9. ESI-TOF-MS spectra of **2d** in CH_2Cl_2.
Figure S10. ESI-TOF-MS spectra of **3a** in CH_2Cl_2.
Figure S11. $^{31}P\{^1H\}$ NMR spectrum of **3a** in CD_2Cl_2.
Figure S12. DFT full-optimized structures of (a) **1a** and (d) **2d** by B3LYP methods with lanl2dz.
Figure S13. Representative MO diagrams for the DFT optimized structure of (a) **1a** and (b) **2d** by B3LYP methods with lanl2dz.
Figure S14. Natural population analyses, natural charge and Wiberg bond indices, for the DFT optimized structures of (a) **1a** and (b) **2d** by B3LYP methods with lanl2dz.

Experimental and spectral data for complexes 1a–c and **2a–d**

General procedure for the synthesis of 1a–c

To a solution of dpmppp in dichloromethane (10 mL) was added 1 eq. of $[RhCl(cod)]_2$ and 1 eq. of RNC, and the reaction mixture was stirred at room temperature for 12 h. The solvent was removed under reduced pressure to dryness and the residue was washed with Et_2O (5 mL × 3) and acetone (3 mL × 1) and extracted with 10 mL of dichloromethane. The extract was concentrated to ca. 3 mL. After addition of diethyl ether, the solution was allowed to stand at room temperature to afford pale orange crystals of **1a–c**.

$[Rh_2Cl_2(dpmppp)(XylNC)]\cdot Et_2O\cdot 0.5CH_2Cl_2$ (1a). Yield: 180 mg, 74% from dpmppp (0.169 mmol). Anal. Calcd for $C_{55.5}H_{62}Cl_5NOP_4Rh_2$: C, 52.65; H, 4.94; N, 1.10. Found: C, 52.83; H, 5.05; N, 1.37. IR (KBr): ν 2058 (s), 1434 (s), 1098 (s), 743 (m), 718 (m), 694 (m) cm^{-1}. ESI-MS (CH_2Cl_2): *m/z* 1028.02 (*z*1, $[Rh_2Cl(dpmppp)(XylNC)]^+$ (1028.06)). ^1H NMR (CD_2Cl_2): δ 1.1 (m, 1H, CH_2), 1.67 (s, 6H, *o*-Me (Xyl)), 2.0 (m, 1H, CH_2), 2.28 (brs, 4H, CH_2), 3.41 (m, 2H, CH_2), 4.72 (m, 2H, CH_2), 6.78-8.04 (m, 33H, Ph). $^{31}P\{^1H\}$ NMR (CD_2Cl_2): δ 15.6 (dt, 2P, $1J_{PRh}$ = 134 Hz, $^2J_{PP}$ = 38 Hz, P_{out}), 21.0 (dt, 2P, $^1J_{PRh}$ = 143 Hz, $^2J_{PP}$ = 35 Hz, P_{in}).

$[Rh_2Cl_2(dpmppp)(DipNC)]\cdot 0.5CH_2Cl_2$ (1b). Yield: 54.2 mg, 64% from dpmppp (0.075 mmol). Anal. Calcd for $C_{54.5}H_{58}Cl_3NP_4Rh_2$: C, 56.28; H, 5.03; N, 1.20. Found: C, 56.24; H, 4.71; N, 1.25. IR (KBr): ν 2051 (s), 1434 (s), 1097 (s), 742 (m), 717 (m), 693 (m) cm^{-1}. ESI-MS (CH_2Cl_2): *m/z* 1084.09 (*z*1, $[Rh_2Cl(dpmppp)(DipNC)]^+$ (1084.12)). ^1H NMR (CD_2Cl_2): δ 0.71 (d, 12H, Me (^{i}Pr), *J* = 7 Hz), 1.10 (m, 1H, CH_2), 2.00 (m, 1H, CH_2), 2.22 (brs, 4H, CH_2), 2.53 (7, 2H, CH (iPr)), 3.44 (m, 2H, CH_2), 4.71 (m, 2H, CH_2), 6.85-8.03 (m, 33H, Ph). $^{31}P\{^1H\}$ NMR (CD_2Cl_2): δ 15.6 (dt, 2P, $^1J_{PRh}$ = 131 Hz, $^2J_{PP}$ = 36 Hz, P_{out}), 21.0 (dt, 2P, $^1J_{PRh}$ = 143 Hz, $^2J_{PP}$ = 36 Hz, P_{in}).

$[Rh_2Cl_2(dpmppp)(MesNC)]\cdot CH_2Cl_2$ (1c). Yield: 98.3 mg, 61% from dpmppp (0.091 mmol). Anal. Calcd for $C_{52}H_{53}Cl_4NP_4Rh_2$: C, 53.68; H, 4.59; N, 1.20. Found: C, 53.50; H, 4.82; N, 1.10. IR (KBr): ν 2043 (s), 1433 (s), 1099 (s), 740 (m), 722 (m), 693 (m) cm^{-1}. ESI-MS (CH_2Cl_2): *m/z* 1042.15 (*z*1, $[Rh_2Cl(dpmppp)(MesNC)]^+$ (1042.08)). ^1H NMR (CD_2Cl_2): δ 1.10 (m, 1H, CH_2), 1.62 (s, 6H, *o*-Me (Mes)), 2.0 (m, 1H, CH_2), 2.12 (s, 4H, *p*-Me (Mes)), 2.27 (s, 4H, CH_2), 3.39 (m, 2H, CH_2), 4.71 (m, 2H, CH_2), 6.60-8.04 (m, 32H, Ph). $^{31}P\{^1H\}$ NMR (CD_2Cl_2): δ 15.5 (dt, 2P, $^1J_{PRh}$ = 133 Hz, $^2J_{PP}$ = 40, 35 Hz, P_{out}), 21.1 (dt, 2P, $^1J_{PRh}$ = 143 Hz, $^2J_{PP}$ = 38, 35Hz, P_{in}).

General procedure for the synthesis of 2a–c

The solution of **1a–c** in CD_2Cl_2 (0.4 mL) was placed at -15 ^oC and reaction progress was monitored by $^{31}P\{^1H\}$ NMR. After 24 h, **2a–c** were formed in quantitative yields. Solvent was removed under reduced pressure to dryness to give the mixture of **2** and **1** with the ration of ca 9 : 1, which were used for IR measurements.

[$Rh_2Cl_2(O_2)$(dpmppp)(XylNC)] (2a).

IR (KBr): ν 2136 (s), 1434 (s), 1096 (m), 803 (m), 742 (m), 719 (m) cm^{-1}. ESI-MS (CH_2Cl_2): *m/z* 1060.08 (*z*1, $[Rh_2Cl(O_2)(dpmppp)(XylNC)]^+$ (1060.05)). ^1H NMR (CD_2Cl_2): δ 1.20-1.32 (m, 1H, CH_2), 1.98 (s, 6H, *o*-Me (Xyl)), 2.00 (m, 1H, CH_2), 2.45 (m, 2H, CH_2), 2.94 (m, 2H, CH_2), 3.48 (m, 2H, CH_2), 4.71 (m, 2H, CH_2), 6.95-8.14 (m, 33H, Ph). $^{31}P\{^1H\}$ NMR (CD_2Cl_2): δ 9.6 (dt, 2P, $^1J_{PRh}$ = 96 Hz, $^2J_{PP}$ = 32 Hz, P_{out}), 27.6 (dt, 2P, $^1J_{PRh}$ = 136 Hz, $^2J_{PP}$ = 32 Hz, P_{in}).

[$Rh_2Cl_2(O_2)$(dpmppp)(DipNC)] (2b).

IR (KBr): ν 2137 (s), 1438 (s), 1098 (m), 741 (m), 715 (m) cm^{-1}. ESI-MS (CH_2Cl_2): *m/z* 1116.20 (*z*1, $[Rh_2Cl(O_2)(dpmppp)(DipNC)]^+$ (1116.11)). ^1H NMR (CD_2Cl_2): δ 0.97 (s, 12H, Me (^{i}Pr)), 1.20-1.32 (m, 1H, CH_2), 2.02 (m, 1H, CH_2), 2.46 (m, 2H, CH_2), 2.95 (m, 2H, CH_2), 3.36 (m, 2H, CH (^{i}Pr)), 3.46 (m, 2H, CH_2), 4.56 (m, 2H, CH_2), 6.80-8.40 (m, 33H, Ph). $^{31}P\{^1H\}$ NMR (CD_2Cl_2): δ 11.3 (dt, 2P, $^1J_{PRh}$ = 97 Hz, $^2J_{PP}$ = 32 Hz, P_{out}), 27.5 (dt, 2P, $^1J_{PRh}$ = 136 Hz, $^2J_{PP}$ = 33 Hz, P_{in}).

[$Rh_2Cl_2(O_2)$(dpmppp)(MesNC)] (2c).

IR (KBr): ν 2137 (s), 1435 (m), 1098 (m) cm^{-1}. ESI-MS (CH_2Cl_2): *m/z* 1074.17 (*z*1, $[Rh_2Cl(O_2)(dpmppp)(MesNC)]^+$ (1074.07)). ^1H NMR (CD_2Cl_2): δ 1.20-1.32 (m, 1H, CH_2), 1.94 (s, 6H, *o*-Me (Mes)), 2.01 (m, 1H, CH_2), 2.27 (s, 3H, *p*-Me (Mes)), 2.46 (m, 2H, CH_2), 2.95 (m, 2H, CH_2), 3.47 (m, 2H, CH_2), 4.72 (m, 2H, CH_2), 6.70-8.10 (m, 32H, Ph). $^{31}P\{^1H\}$ NMR (CD_2Cl_2): δ 9.4 (dt, 2P, $^1J_{PRh}$ = 97 Hz, $^2J_{PP}$ = 34 Hz, P_{out}), 27.5 (dt, 2P, $^1J_{PRh}$ = 136 Hz, $^2J_{PP}$ = 35 Hz, P_{in}).

Crystals of **2c** suitable for X-ray analysis was obtained by recrystallization from CH_3CN / Et_2O.

[$Rh_2Cl_2(O_2)$(dpmppp)(^{t}BuNC)] (2d).

To a solution of $[Rh_3Cl_3(dpmppp)(CO)_2]$ (17.0 mg, 0.015 mmol) in CH_2Cl_2 (10 mL) was added ^{t}BuNC. The mixture was concentrated to ca. 3mL. After addition of Et_2O, the solution was stored at -15 ^oC to afford red precipitates, which was removed by

filtration. The filtrate was allowed to stand at room temperature under air to give red crystals of **2d**. Yield: 5 mg, 29%. Anal. Calcd for $C_{54}H_{68}Cl_6NO_{3.5}P_4Rh_2$: C, 48.78; H, 5.16; N, 1.05. Found: C, 48.73; H, 5.06; N, 1.05. IR (KBr): ν 2182 (s), 1434 (s), 1099 (s), 861 (w), 742 (m), 721 (m), 694 (m) cm^{-1}. ESI-MS (CH_2Cl_2): *m/z* 1012.45 (*z*1, $[Rh_2Cl(dpmppp)(^tBuNC)]^+$ (1012.05)). ^1H NMR (CD_2Cl_2): δ 0.83 (s, 9H, Me (^{t}Bu)), 1.30 (m, 1H, CH_2), 2.15 (m, 1H, CH_2), 2.51 (m, 2H, CH_2), 2.96 (m, 2H, CH_2), 3.33 (m, 2H, CH_2), 5.07 (m, 2H, CH_2), 7.20-8.14 (m, 30H, Ph). $^{31}P\{^1H\}$ NMR (CD_2Cl_2): δ 5.8 (dt, 2P, $^1J_{PRh}$ = 97 Hz, $^2J_{PP}$ = 33 Hz, P_{out}), 27.3 (dt, 2P, $^1J_{PRh}$ = 143 Hz, $^2J_{PP}$ = 35 Hz, P_{in}).

Reaction of 2a with HCl in the presence of PPh_3.

After a solution of **1a** (8.2 mg, 7.7 μmol) in CD_2Cl_2 (0.4 ml) was kept for 24 h at -15 °C under air, **2a** was formed quantitatively, which was confirmed by $^{31}P\{^1H\}$ NMR. To the solution, HCl in Et_2O (1.0 M, 23.1 μl, 23.1 μmol) and PPh_3 (2.0 mg, 7.6 μmol) were added succesively at room temperature to form $[Rh_2Cl_4(dpmppp)(XylNC)]$ (**3a**) and $Ph_3P{=}O$ in 95 and 75% yields, respectively.

3a: IR (KBr): ν 2167 (s), 1435 (s), 1098 (s), 739 (m), 691 (m) cm^{-1}. ESI-MS (CH_2Cl_2): *m/z* 1098.02 (*z*1, $[Rh_2Cl_3(dpmppp)(XylNC)]^+$ (1098.00)), 966.95 (*z*1, $[Rh_2Cl_3(dpmppp)]^+$ (966.93)). ^1H NMR (CD_2Cl_2): δ 1.33 (m, 2H, CH_2), 2.01 (m, 2H, CH_2), 3.70 (m, 4H, CH_2), 4.60 (m, 2H, CH_2), 6.93-8.07 (m, 33H, Ph). $^{31}P\{^1H\}$ NMR (CD_2Cl_2): δ 4.6 (dt, 2P, $^1J_{PRh}$ = 90 Hz, $^2J_{PP}$ = 32 Hz, P_{out}), 32.1 (dt, 2P, $^1J_{PRh}$ = 135 Hz, $^2J_{PP}$ = 31 Hz, P_{in}).

X-ray Crystallography. The crystals of **1a**·$3CH_2Cl_2$, **1b**·$2Me_2CO$, **2c**·4MeNC·$0.5H_2O$ and **2d**·CH_2Cl_2 suitable for X-ray analyses were quickly coated with Paratone N oil and mounted on top of a loop fiber at room temperature. Crystal and experimental data are summarized in Tables S1–2. All data were collected at –120 °C on a Rigaku AFC8R/Mercury CCD diffractometer equipped with graphite-monochromated Mo Kα radiation using a rotating-anode X-ray generator (50 kV, 180 mA) and a Rigaku VariMax Mo/Saturn CCD diffractometer equipped with graphite-monochromated Mo Kα radiation using a rotating-anode X-ray generator RA-Micro7 (50 kV, 24 mA). A total of 1440 for **1a**, **1b**, **2c** and 2160 for **2d** oscillation images, covering a whole sphere of $6° < 2\theta < 55°$ were corrected by ω–scan method. The crystal-to-detector (70 × 70 mm) distance was set at 45 or 60 mm. The data were processed using the *Crystal Clear 1.3.5* program (Rigaku/MSC)[1] and corrected for

Lorentz–polarization and absorption effects.[2] The structures of complexes were solved by direct methods with SHELXS-97[3] (**2d**) and SIR-92[4] (**1a**, **1b**, **2c**), and were refined on F^2 with full-matrix least-squares techniques with SHELXL-97[3] using *Crystal Structure 4.0* package.[5] All non-hydrogen atoms were refined with anisotropic thermal parameters, and the C-H hydrogen atoms were calculated at ideal positions and refined with riding models. All calculations were carried out on a Windows PC with *Crystal Structure 4.0* package.[5]

In the structure of **1a**, the solvated two CH_2Cl_2 molecules are distorted with two sites for each molecule and the populations were refined as C52/C53 = Cl7/Cl6 = 0.53/0.47 and C54/C55 = Cl9/Cl10 = 0.58/0.42. The distorted molecules were refined anisotropically with constrained and fvar techniques. In **2c**, the SQUEEZE program of the PLATON suite found a void of 146 $Å^3$ at (0, 0, 0.5) and removed 17 e^-, corresponding to a MeCN/cell. This molecule could not be located owing to disorder. However, this molecule is included in the empirical formula and calculations based on it.

References

1) *Crystal Clear, version 1.3.5; Operating software for the CCD detector system*, Rigaku and Molecular Structure Corp., Tokyo, Japan and The Woodlands, Texas, 2003.
2) Jacobson, R. *REQAB*; Molecular Structure Corporation: The Woodlands, Texas, USA, 1998.
3) Sheldrick, G. M. *SHELXL-97: Program for the Refinement of Crystal Structures.* University of Göttingen, Göttingen, Germany, 1996.
4) Altomare, A.; Burla, M. C.; Camalli, M.; Cascarano, M.; Giacovazzo, C.; Guagliardi, A.; Polidori, G. *J. Appl. Cryst.* **1994**, *27*, 435-436.
5) *CrystalStructure 4.0*: Crystal Structure Analysis Package, Rigaku Corporation (2000-2010). Tokyo 196-8666, Japan.

Table S1. Crystallographic Data of Complexes 1a·3CH_2Cl_2, 1b·2Me_2CO, 2c·4.5MeNC and 2d·CH_2Cl_2

Compound	**1a**·3CH_2Cl_2	**1b**·2Me_2CO	**2c**·4.5MeNC	**2d**·CH_2Cl_2
formula	$C_{53}H_{55}Cl_8NP_4Rh_2$	$C_{60}H_{69}NO_2P_4Rh_2$	$C_{60}H_{64.5}Cl_2N_{5.5}O_2P_4Rh_2$	$C_{47}H_{51}Cl_4NO_2P_4Rh_2$
formula wt	1319.35	1236.82	1295.32	1133.44
cryst. syst	monoclinic	monoclinic	triclinic	orthorhombic
space group	$P2_1/n$	$P2_1/n$	$P\bar{1}$	$Pna2_1$
a, Å	13.404(7)	13.687(5)	12.604(6)	29.706(15)
b, Å	14.372(8)	14.485(6)	12.861(5)	14.423(7)
c, Å	30.132(12)	29.226(11)	20.226(9)	11.405(6)
α, deg			73.940(7)	
β, deg	95.9511(12)	91.683(6)	80.980(6)	
γ, deg			74.474(7)	
V, Å^3	5773(5)	5792(4)	3023(3)	4887(4)
Z	4	4	2	4
temp, °C	-120	-120	-120	-120
D_{calcd}, g cm^{-1}	1.518	1.418	1.423	1.541
μ, mm^{-1} (Mo Kα)	1.086	0.813	0.784	1.061
F(000)	2664	2544	1326	2296
2θ range, deg	6–55	6–55	6–55	6–55
R_{int}	0.050	0.052	0.051	0.065
no. of reflns collected	54025	66152	35608	42551
no. of unique reflns	13226	13179	13775	10915
no. of obsd reflns ($I > 2\sigma(I)$)	11658	10861	10071	9275
no. of variables	651	648	674	542
*R*1[a]	0.056	0.059	0.064	0.067
*wR*2[b]	0.147	0.155	0.193	0.183
GOF	1.086	1.159	1.069	1.067
Flack Parameter				0.08(4)
CCDC number	CCDC 928791	CCDC 928792	CCDC 928793	CCDC 928794

[a] $R1 = \Sigma\big||F_o| - |F_c|\big|/\Sigma|F_o|$ (for obsd. refs with $I > 2\sigma(I)$). [b] $wR2 = [\Sigma w(F_o^2 - F_c^2)^2/\Sigma w(F_o^2)^2]^{1/2}$ (for all refs).

Table S2. Structural Parameters of 1a, 1b, 2c and 2d.[a]

	1a	**1b**	**2c**	**2d**
Rh1–Rh2	2.6873(10)	2.6949(10)	2.7455(10)	2.7637(7)
Rh1–Cl1	2.3845(14)	2.4179(14)	2.4016(17)	2.4278(19)
Rh1–Cl2	2.4030(15)	2.3864(13)	2.4121(16)	2.412(2)
Rh1–P2	2.2034(15)	2.1993(12)	2.1928(16)	2.2259(19)
Rh1–P3	2.2027(14)	2.2074(13)	2.2026(16)	2.2112(19)
Rh2–P1	2.3095(14)	2.3002(13)	2.3472(14)	2.363(2)
Rh2–P4	2.2951(15)	2.3061(12)	2.3649(14)	2.3650(19)
Rh2–C1	1.844(4)	1.864(5)	1.927(6)	1.950(8)
Rh2–O1			2.016(5)	2.039(5)
Rh2–O2			2.026(4)	2.021(5)
C1-N1	1.169(6)	1.164(6)	1.158(7)	1.189(10)
O1–O2			1.436(4)	1.449(7)
Rh1–Rh2–O1			114.83(9)	118.64(14)
Rh1–Rh2–O2			156.41(10)	160.44(15)
O1-Rh1-O2			41.63(13)	41.8(2)
Rh1–Rh2–C1	172.79(13)	167.97(14)	83.14(13)	79.7(2)
Cl1–Rh1–Cl2	89.50(5)	89.91(4)	89.52(5)	88.96(6)
P2–Rh1–P3	95.10(5)	94.41(5)	94.46(6)	93.59(6)
P1–Rh2–P4	170.89(4)	167.19(4)	170.41(6)	172.40(7)

[a] The atomic numbering schemes are shown in Figures 1, 4, S1 and S2.

Figure S1. ORTEP diagram for **1b** with the atomic numbering scheme. The thermal ellipsoids are drawn at the 40% probability level, and the hydrogen atoms are omitted for clarity.

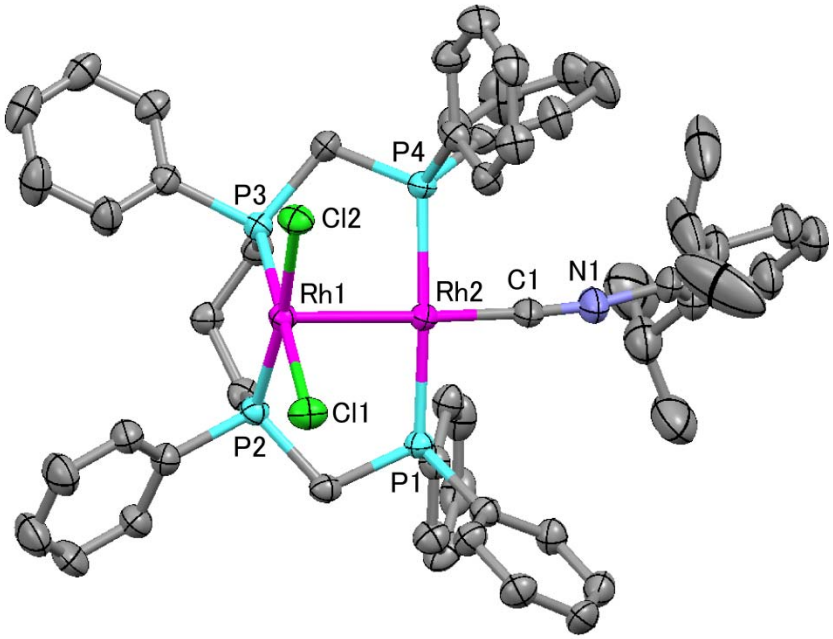

Figure S2. ORTEP diagram for **2c** with the atomic numbering scheme. The thermal ellipsoids are drawn at the 40% probability level, and the hydrogen atoms are omitted for clarity.

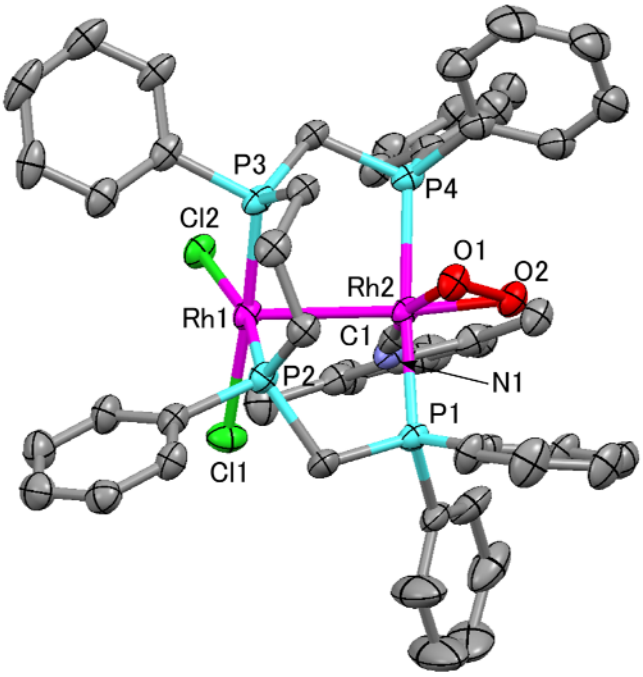

Figure S3. ESI-TOF-MS spectra of **1a** in CH_2Cl_2.

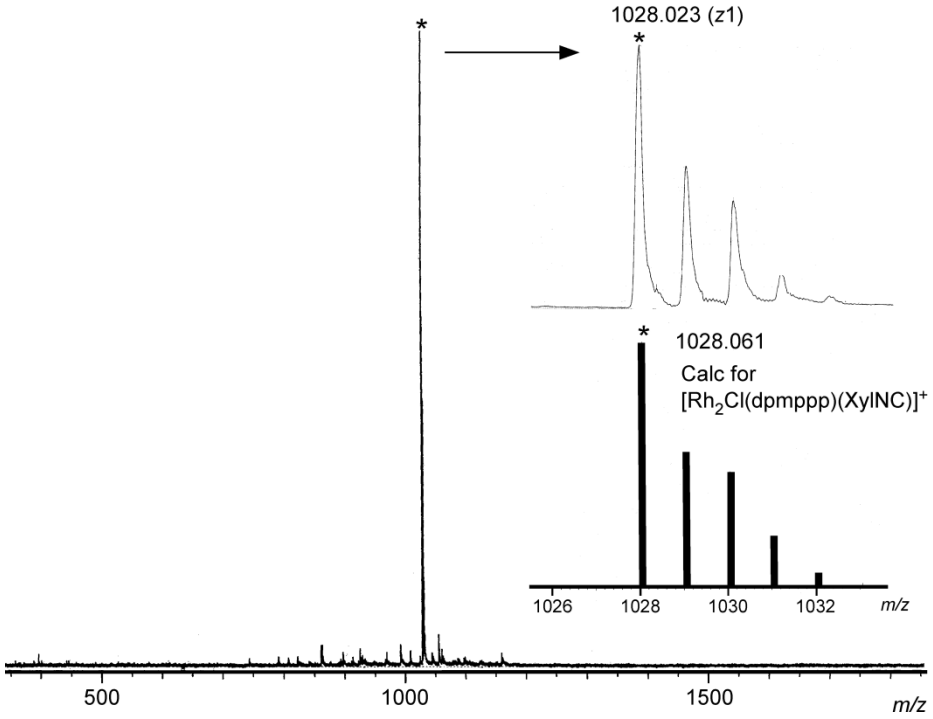

Figure S4. ESI-TOF-MS spectra of **1b** in CH_2Cl_2.

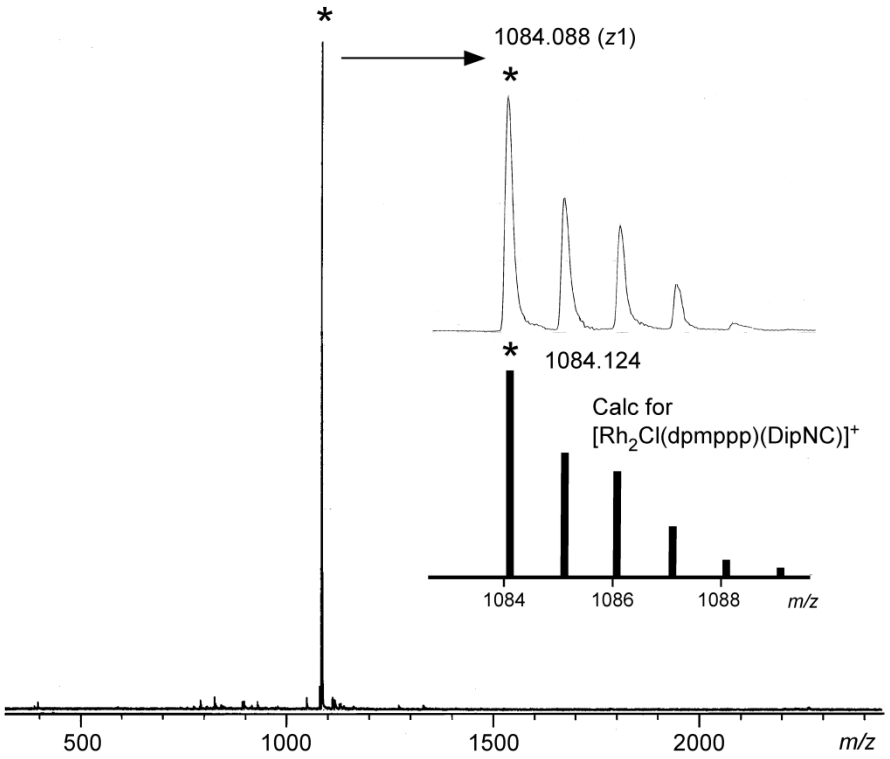

Figure S5. ESI-TOF-MS spectra of **1c** in CH_2Cl_2.

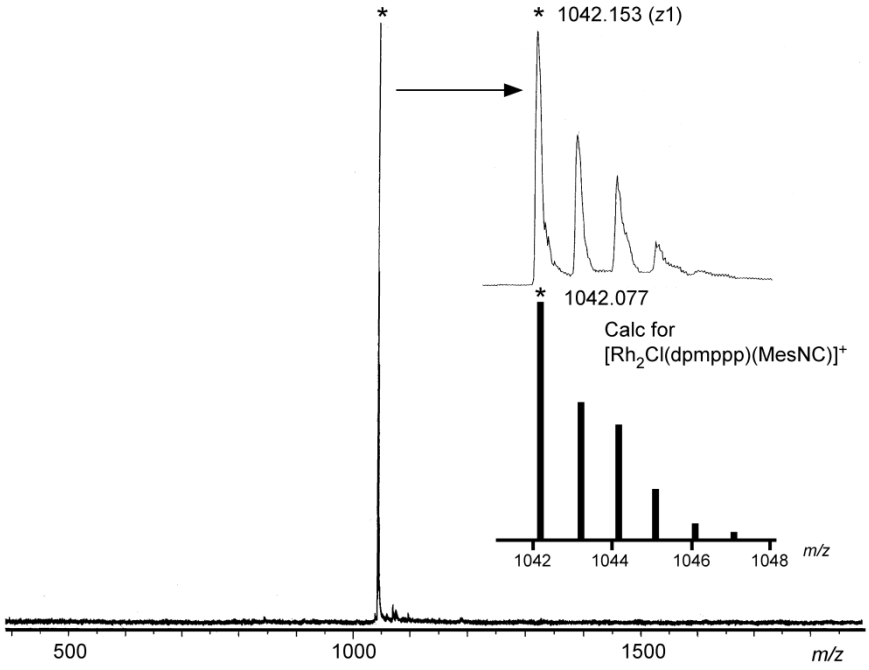

Figure S6. ESI-TOF-MS spectra of **2a** in CH_2Cl_2.

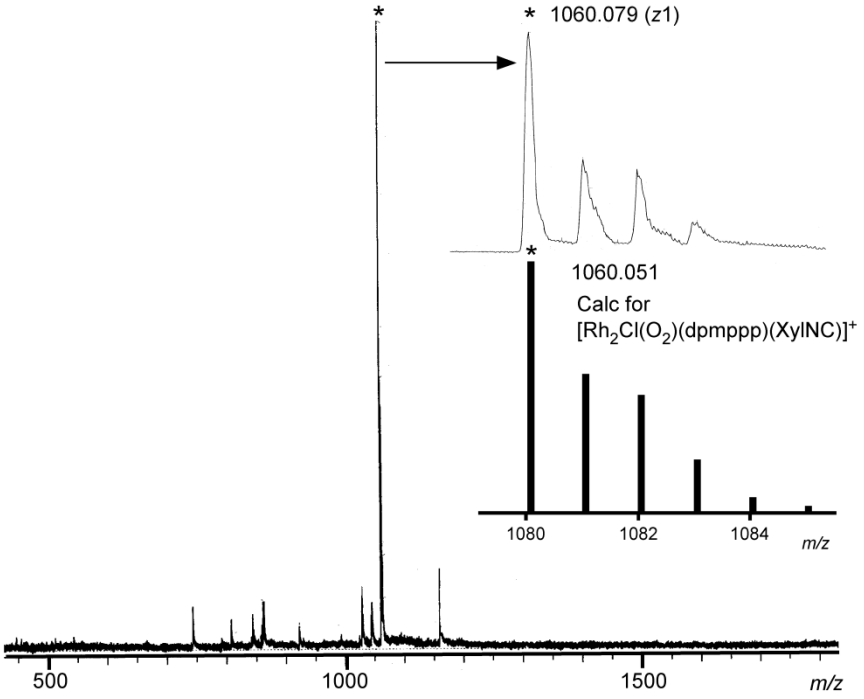

Figure S7. ESI-TOF-MS spectra of **2b** in CH_2Cl_2.

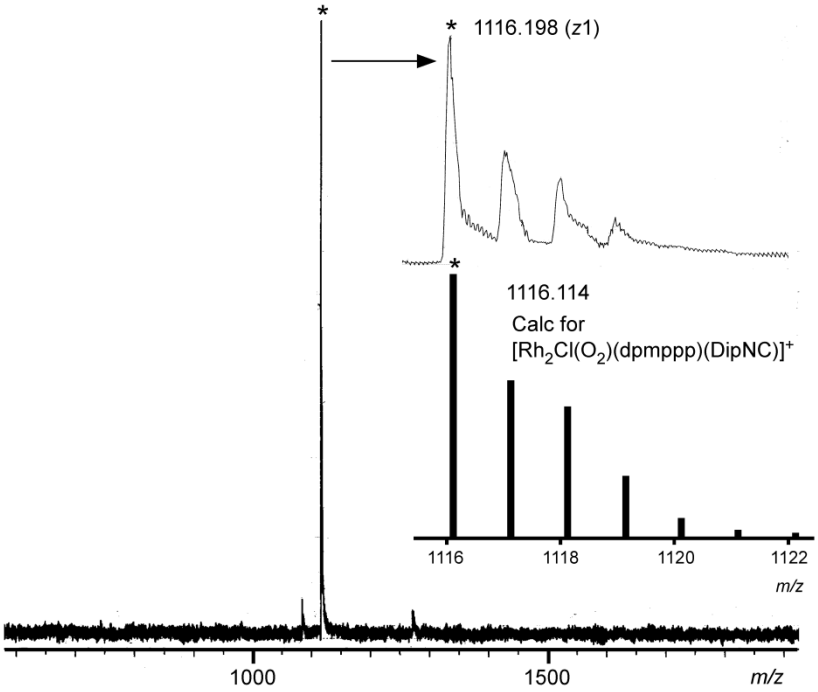

Figure S8. ESI-TOF-MS spectra of **2c** in CH_2Cl_2.

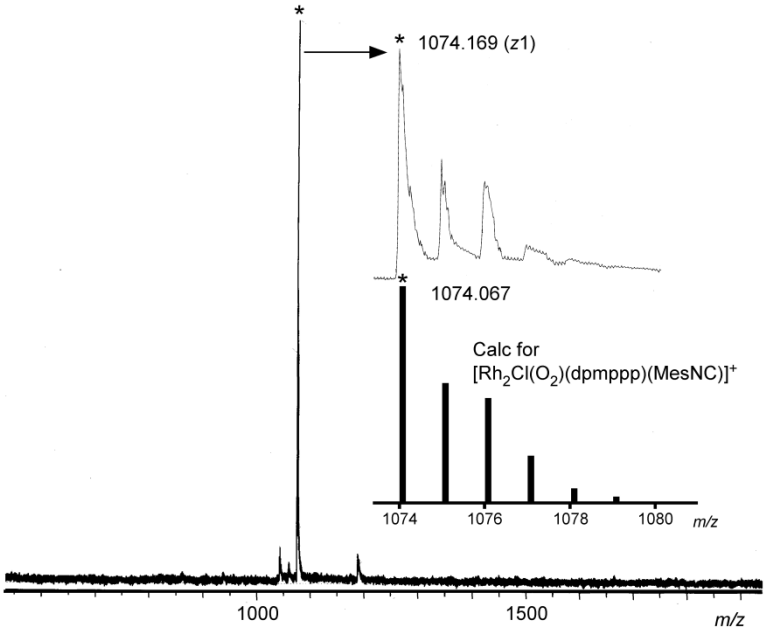

Figure S9. ESI-TOF-MS spectra of **2d** in CH_2Cl_2.

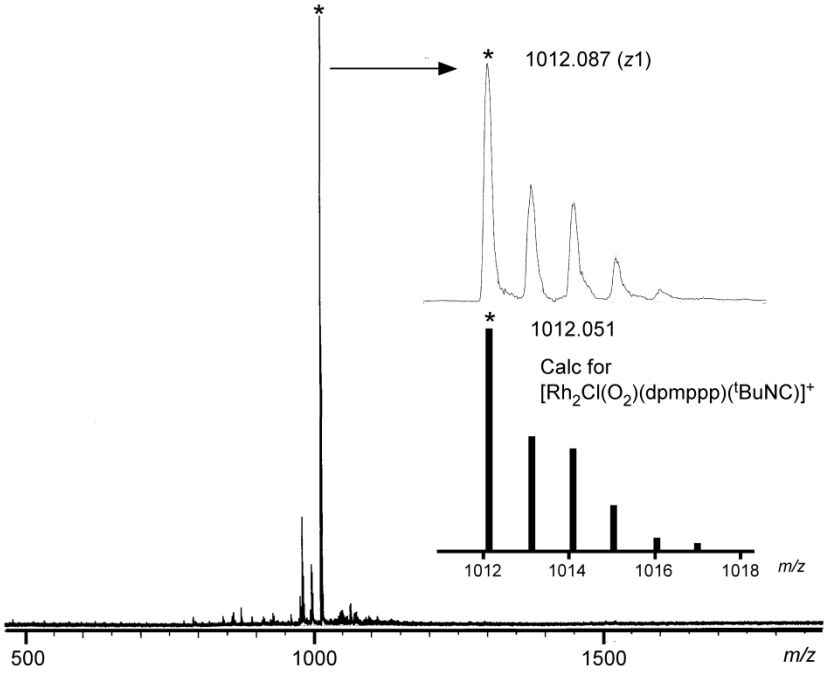

Figure S10. ESI-TOF-MS spectra of **3a** in CH_2Cl_2.

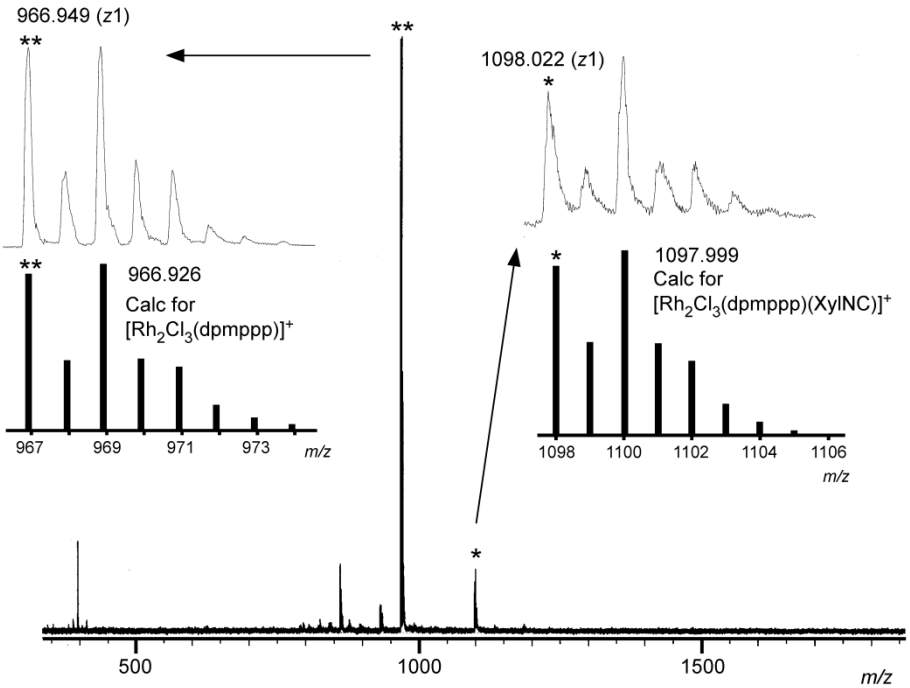

Figure S11. $^{31}P\{^{1}H\}$ NMR spectrum of **3a** in CD_2Cl_2.

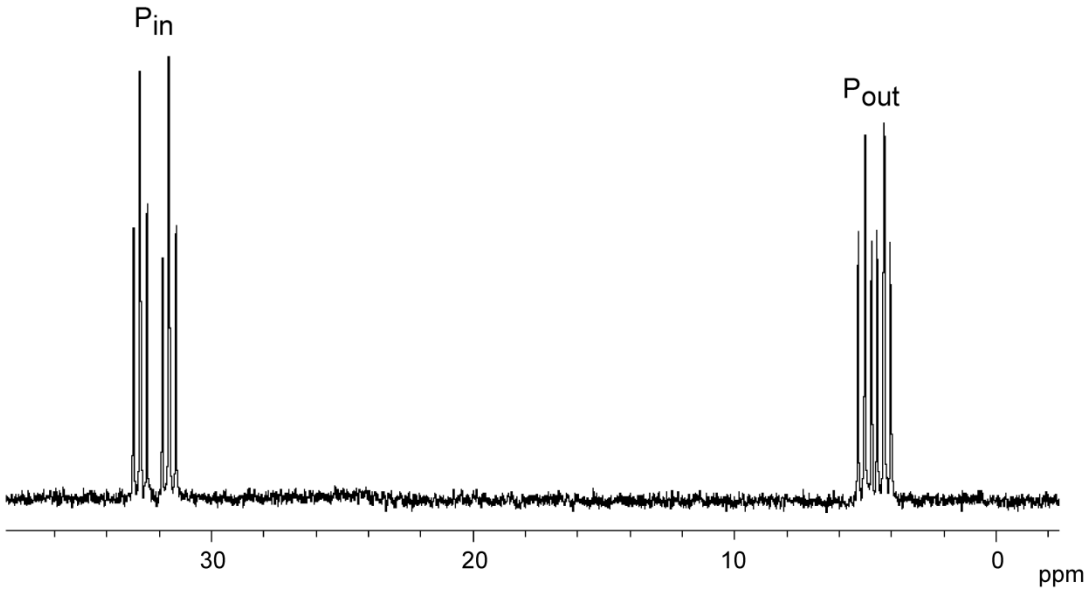

Figure S12. DFT full-optimized structures of (a) **1a** and (d) **2d** by B3LYP methods with lanl2dz.

(a)

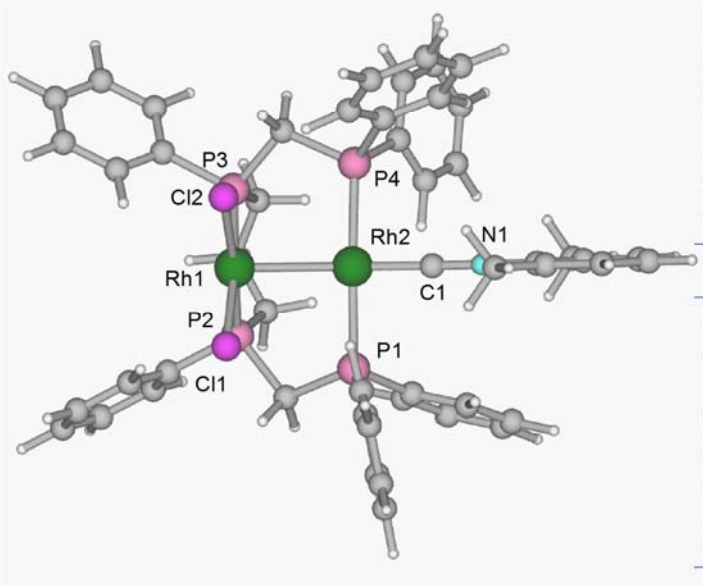

Distance (Å)	DFT	X-ray
Rh1–Rh2	2.7654	2.6873(10)
Rh1–Cl1	2.459	2.385(1)
Rh1–Cl2	2.466	2.403(2)
Rh1–P2	2.328	2.203(2)
Rh1–P3	2.333	2.203(1)
Rh2–P1	2.421	2.310(2)
Rh2–P4	2.422	2.295(2)
Rh2–C1	1.892	1.844(2)
N1–C1	1.199	1.169(6)

Angle (°)	DFT	X-ray
Rh2–Rh1–P2	86.63	83.51(3)
Rh2–Rh1–P3	88.47	85.90(3)
Rh2–Rh1–Cl1	96.81	101.45(3)
Rh2–Rh1–Cl2	97.79	99.71(3)
P2–Rh1–P3	94.98	95.10(5)
Rh1–Rh2–C1	167.36	172.79(13)
Rh1–Rh2–P1	90.45	89.20(3)
Rh1–Rh2–P4	91.97	93.83(3)
P1–Rh2–P4	167.53	170.89(4)

(b)

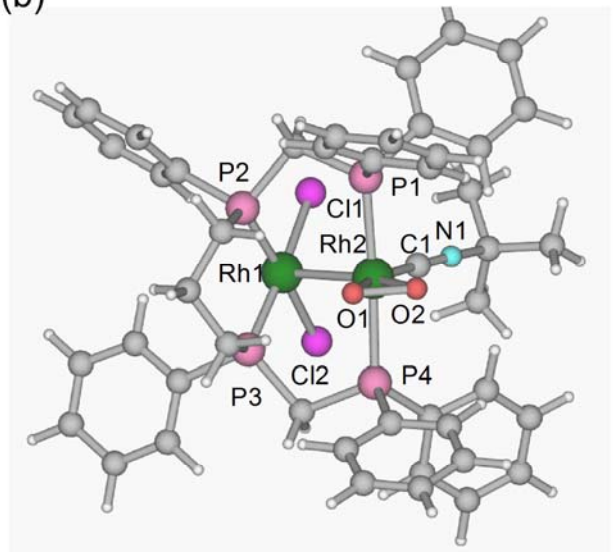

Distance (Å)	DFT	X-ray
Rh1–Rh2	2.8055	2.7637(7)
Rh1–Cl1	2.480	2.428(2)
Rh1–Cl2	2.473	2.412(2)
Rh1–P2	2.343	2.226(2)
Rh1–P3	2.341	2.211(2)
Rh2–P1	2.457	2.363(2)
Rh2–P4	2.454	2.365(2)
Rh2–C1	1.968	1.950(8)
Rh2–O1	2.077	2.039(5)
Rh2–O2	2.085	2.021(5)
N1–C1	1.181	1.189(6)
O1–O2	1.483	1.449(7)

Angle (°)	DFT	X-ray	Angle (°)	DFT	X-ray
Rh2–Rh1–P2	85.23	84.73(4)	Rh1–Rh2–C1	83.74	79.7(2)
Rh2–Rh1–P3	85.07	83.33(5)	Rh1–Rh2–O1	113.29	118.64(14)
Rh2–Rh1–Cl1	99.35	103.88(5)	Rh1–Rh2–O2	155.03	160.44(15)
Rh2–Rh1–Cl2	100.31	100.45(5)	Rh1–Rh2–P1	91.82	92.04(5)
P2–Rh1–P3	93.78	93.59(6)	Rh1–Rh2–P4	91.88	90.23(4)
			P1–Rh2–P4	168.97	172.40(7)
			O1–Rh2–O2	41.74	41.8(2)

Figure S13. Representative MO diagrams for the DFT optimized structure of (a) **1a** and (b) **2d** by B3LYP methods with lanl2dz.

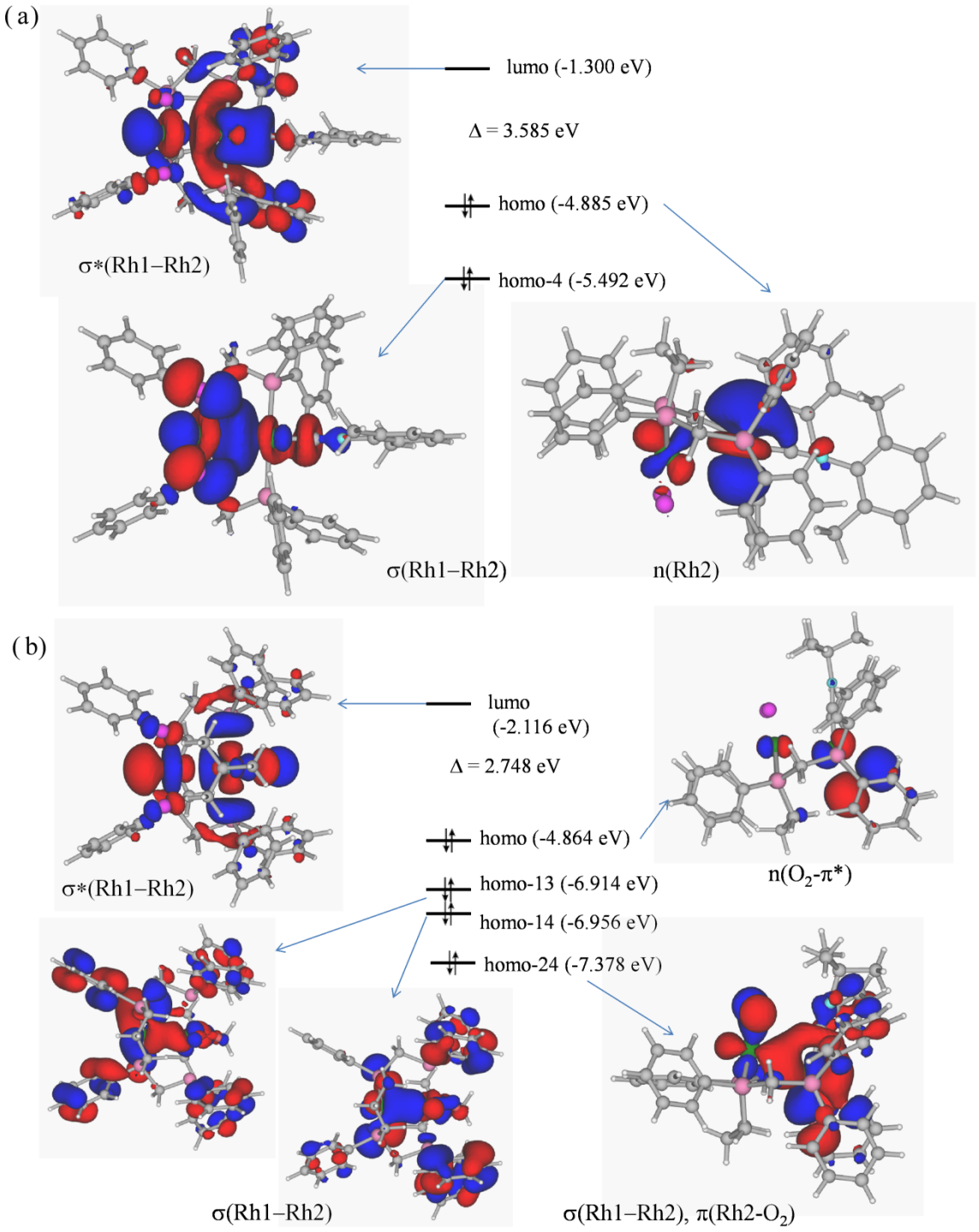

Figure S14. Natural population analyses, natural charge and Wiberg bond indices, for the DFT optimized structures of (a) **1a** and (b) **2d** by B3LYP methods with lanl2dz.